Peptaibol Zervamicin IIB Structure and Dynamics Refinement from Transhydrogen Bond *J* Couplings

Z. O. Shenkarev, T. A. Balashova, Z. A. Yakimenko, T. V. Ovchinnikova, and A. S. Arseniev
Shemyakin-Ovchinnikov Institute of Bioorganic Chemistry, Russian Academy of Sciences, Moscow, Russia

ABSTRACT   Zervamicin IIB (Zrv-IIB) is a channel-forming peptaibol antibiotic of fungal origin. The measured transhydrogen bond $^{3h}J_{NC'}$ couplings in methanol solution heaving average value of -0.41 Hz indicate that the stability of the Zrv-IIB helix in this milieu is comparable to the stability of helices in globular proteins. The N-terminus of the peptide forms an α-helix, whereas 3_{10}-helical hydrogen bonds stabilize the C-terminus. However, two weak transhydrogen bond peaks are observed in a long-range HNCO spectrum for HN Aib^{12}. Energy calculations using the Empirical Conformation Energy Program for Peptides (ECEPP)/2 force field and the implicit solvent model show that the middle of the peptide helix accommodates a bifurcated hydrogen bond that is simultaneously formed between HN Aib^{12} and CO Leu^8 and CO Aib^9. Several lowered $^{3h}J_{NC'}$ on a polar face of the helix correlate with the conformational exchange process observed earlier and imply dynamic distortions of a hydrogen bond pattern with the predominant population of a properly folded helical structure. The refined structure of Zrv-IIB on the basis of the observed hydrogen bond pattern has a small ($\sim20°$) angle of helix bending that is virtually identical to the angle of bending in dodecylphosphocholine (DPC) micelles, indicating the stability of a hinge region in different environments. NMR parameters (^{1}HN chemical shifts and transpeptide bond $^{1}J_{NC'}$ couplings) sensitive to hydrogen bonding along with the solvent accessible surface area of carbonyl oxygens indicate a large polar patch on the convex side of the helix formed by three exposed backbone carbonyls of Aib^7, Aib^9, and Hyp^{10} and polar side chains of Hyp^{10}, Gln^{11}, and Hyp^{13}. The unique structural features, high helix stability and the enhanced polar patch, set apart Zrv-IIB from other peptaibols (for example, alamethicin) and possibly underlie its biological and physiological properties.

INTRODUCTION

Ion channels are large transmembrane machines, which allow ions to flow through cell membranes with colossal speed and impressive selectivity at the same time. They play a key role in all aspects of the cell functioning, especially in signal transduction. Due to the extremely large size of the naturally occurring ion channels, they represent a challenge for structural investigation with atomic precision. Although some progress in studying of voltage-gated channels by x-ray crystallography was made, our knowledge about their functional principles is still very poor (Doyle et al., 1998; Jiang et al., 2002b, 2003a).

Nature provides us with the diverse family of so-called channel-forming peptides (CFPs), which can reproduce some properties of large cell ion channels (Sansom, 1991). One of the most extensively studied groups of channel-forming peptides is peptaibols, which represent a subfamily of small (7–24 amino acids) helical peptide antibiotics of fungal origin (Duclohier and Wroblewski, 2001). The peptaibols form voltage-gated channels with multilevel conductance (Sansom, 1991) and possess selectivity toward monovalent cations (Hanke and Boheim, 1980).

It is generally thought that an active peptaibol channel is represented by a bundle of parallel transmembrane helices (barrel-stave model) (Baumann and Mueller, 1974; He et al.,

1995; Tieleman et al., 2002). A similar molecular organization is observed in membrane components of large ion channels (Doyle et al., 1998; Jiang et al., 2002a, 2003a). In this respect, peptaibols can be considered a simple model of naturally occurring ion channels (Wallace, 2000) and may shed light upon general mechanism of ion channel functioning.

The most discussed questions regarding peptaibols are structures of the active channels (Tieleman et al., 2002) and mechanisms of their functioning, particularly reasons for the ion selectivity and principles of the voltage gating (Sansom, 1991; Barranger-Mathys and Cafiso, 1996; Tieleman et al., 2001a). Based on the alamethicin studies, it is broadly speculated that exposed backbone carbonyls in the middle of the peptaibol helix may play a significant role in the ion conductance through the channel (Fox and Richards, 1982; Sansom, 1991; Sansom et al., 1993; Wallace, 2000). There is no consensus about the mechanism of the peptaibol voltage gating, which is usually attributed either to the voltage-driven conformational changes at the C-terminus of the peptaibol molecule (Fox and Richards, 1982; North et al., 1994; Franklin et al., 1994; Yee et al., 1995; Tieleman et al., 2001b) or to the voltage-driven insertion of the molecular helical dipoles into the membrane (Barranger-Mathys and Cafiso, 1996; Tieleman et al., 2001a; Shenkarev et al., 2002).

The object of this study is the peptaibol zervamicin IIB (Zrv-IIB) produced by the fungus *Emericellopsis salmosynnemata* (Argoudelis et al., 1974) and comprised of 16 amino acid residues in the following sequence:

AcTrp[1]-Ile[2]-Gln[3]-Iva[4]-Ile[5]-Thr[6]-Aib[7]-Leu[8]-Aib[9]-Hyp[10]-Gln[11]-Aib[12]-Hyp[13]-Aib[14]-Pro[15]-Phl[16] (Ac, N-terminal acetic group; Aib, α-aminoisobutyric acid; Iva, D-iso-valine; Hyp, 4-hydroxyproline; Phl, L-phenylalaninol).

In planar lipid bilayers (Balaram et al., 1992) and vesicular systems (Kropacheva and Raap, 1999, 2002), Zrv-IIB forms voltage dependent ion channels with multilevel conductance states and weak selectivity for Na$^+$. In addition, the Zrv-IIB channel possesses asymmetry; current through the channel is observed in the presence of *cis*-positive potentials only (*cis* denotes the side of the bilayer to which the peptide was added).

In our previous works (Balashova et al., 2000; Shenkarev et al., 2002), the spatial structure of Zrv-IIB was determined in isotropic solvents and bound to dodecylphosphocholine (DPC) micelles. It was shown that in solvents of different polarity, ranging from chloroform/methanol (9:1, v/v) to methanol/water (1:1, v/v), as well as in anisotropic micelles solution, the peptide forms a well-defined bent helix (the angle of bending on Hyp[10] is ~40° in methanol and ~20° in DPC, and the helix length is ~26 Å). Using lipid-soluble spin-labeled probes, it was determined that the peptaibol binds to a surface of DPC micelle with the N-terminus immersed slightly deeper into the micelle interior. Based on these works, the (pre)orientation/insertion model for zerva-micin voltage gating was proposed. In accordance with this model, the gating event involves insertion of the Zrv-IIB monomers into membrane induced by external electric field. This makes the peptaibol conformational changes during the gating event nonessential.

At the same time, recent dynamics investigation of ^{15}N-labeled Zrv-IIB in methanol solution (Korzhnev et al., 2001) demonstrated that the peptide possesses micromillisecond timescale conformational exchange on a polar face of the helix, although it is fairly rigid on a subnanosecond timescale. This conformational exchange along with sub-stantial differences in the angle of the helix bending in various solvents and crystal forms (Karle et al., 1991, 1994) excite interest in more detailed description of the Zrv-IIB dynamics and structure. Additional data are required in order to confidently distinguish between the models of peptaibols voltage gaiting or to suggest a new model for Zrv-IIB functioning.

Here we investigate the hydrogen bond structure and interactions with solvent in ^{13}C,^{15}N-labeled Zrv-IIB. The directly observed hydrogen bond pattern in methanol solution better complies with the pattern proposed for zervamicin in DPC micelles (Shenkarev et al., 2002), rather than with the pattern for zervamicin in methanol proposed previously (Balashova et al., 2000). Presence of two weak transhydrogen bond crosspeaks between HN Aib[12] and CO Leu[8] and CO Aib[9] indicates bifurcated interactions in the middle of the Zrv-IIB helix. The bifurcated hydrogen bonds were never observed in peptaibol structures before (Karle

et al., 1991, 1994, 1998; Snook et al., 1998). Energy calculation using Empirical Conformation Energy Program for Peptides (ECEPP)/2 force field and implicit solvent model also argue in favor of the bifurcated hydrogen bond formed simultaneously between HN Aib[12] and CO Leu[8] and CO Aib[9].

Knowledge of the real hydrogen bond pattern allows us to refine the structure of Zrv-IIB in methanol solution. The refined peptide structure has the angle of the helix bending at Hyp[10] ~20° that better complies with the Zrv-IIB structure in DPC micelles than with the peptide structure in methanol determined previously. The well-defined angle of the helix bending, preserving upon transition to anisotropic micelle environment, along with the strong transhydrogen bond $^{3h}J_{NC'}$ (having an average value of −0.41 ± 0.09 Hz) demonstrate the high stability of the Zrv-IIB helix. This stability is comparable to that of helix regions in globular proteins and restricts the possibility of large amplitude hinge bending motions, peculiar to other peptaibols, for example, to alamethicin (North et al., 1994).

Sites of the weakest $^{3h}J_{NC'}$ correspond to sites of micro-millisecond timescale conformational exchange, and this exchange process involves some distortions of hydrogen bond pattern on a polar face of the helix. Other NMR parameters sensitive to hydrogen bonding (^{1}HN chemical shift and transpeptide bond $^1J_{NC'}$ coupling constants) along with solvent accessible surface area of carbonyl oxygens calculated from the refined structure indicate existence of a polar patch in the middle of the convex face of the Zrv-IIB helix. This patch is formed by the carbonyls of Aib[7], Aib[9], and Hyp[10] with moderate (>6 Å^2 and <15 Å^2) exposure to solvent and by the polar side chains of Hyp[10], Gln[11], and Hyp[13]. This enlarged (as compared to alamethicin) polar patch is possibly the key feature that underlies Na$^+$ selec-tivity of the Zrv-IIB channel.

The unusual rigidity of the Zrv-IIB helix in various en-vironments makes these results also valid for the membrane bound form of the peptide.

MATERIALS AND METHODS

NMR spectroscopy

Uniformly ^{13}C,^{15}N-labeled Zrv-IIB was prepared and purified as described (Ovchinnikova et al., 2003). The sample was dissolved in 0.6 ml deuterated methanol (CD$_3$OH 99.5% deuterium Stohler Isotope Chemicals, Waltham, MA) to the concentration of ~4 mM without adjustment of pH (the direct pH meter reading was 6.2) and was used for NMR experiments. All NMR experiments were carried out on a Bruker (Billerica, MA) DRX-500 spectrometer. The temperature of the sample was 305 K (unless otherwise specified). Spectral assignment was taken from Ovchinnikova et al. (2003).

Carbonyl carbons and amide protons chemical shifts temperature coefficients were measured from the set of HNCO (Grzesiek and Bax, 1992) and HN(CA)CO (Clubb et al., 1992) experiments acquired within the temperature range of 280–320 K. One bond $^1J_{NC'}$ coupling constants across peptide bond were measured from 1D slices of 2D HNCO spectrum obtained without decoupling from ^{13}CO in *t*1 variable delay (without 180° pulse on carbonyls) and processed to a spectral resolution of 0.5 Hz in *f*1.

Detection of hydrogen bond pattern and measurement of $^2J_{NC'}$ (intraresidual) and $^{3h}J_{NC'}$ (across hydrogen bonds) coupling constants were carried out by the method proposed by Cordier and Grzesiek (1999) by means of long-range 2D HNCO experiment at two temperatures, 305 and 315 K. The long-range and reference experiments were acquired with a spectral width of 1.25 kHz × 5 kHz (98 × 1024 complex points) using a 0.7-s interscan delay and with 1024 (long-range) and 16 (reference) scans for each t1 point. Total acquisition times were 66 and 1 h, respectively. Spectra were processed to 256 × 2048 complex points.

To avoid aliasing of aromatic resonances into the carbonyl region of 2D spectra, we used the Gaussian pulse cascades (G3 and G4) (Emsley and Bodenhausen, 1989) as a selective ^{13}CO or $^{13}C^\alpha$ pulses in insensitive nuclei enhanced by polarization transfer (INEPT) steps and t1 variable delay in all HNCO and HN(CA)CO experiments. ^{15}N decoupling during acquisition was achieved using the GARP scheme (Shaka et al., 1985). Quadrature detection in $f1$ direction was done by the States-TPPI method (Marion et al., 1989).

All NMR spectra were processed with Lorenz to Gaussian conversion, linear prediction, and zero filling in the XWINNMR 2.6 (Bruker) program and analyzed in the XEASY program (Bartels et al., 1995).

Structure refinement

The spatial structure calculations were performed using the simulated annealing/molecular dynamics protocol as implemented in the DYANA program, version 1.5 (Guntert et al., 1997). All distance and angle constraints were taken from our previous work (Balashova et al., 2000) without modification. Each hydrogen bond was restrained by four distance restraints; two upper (dH_NO 2.3 Å and dNO 3.3 Å) and two lower (dH_NO 1.8 Å and dNO 2.8 Å), excluding bifurcated hydrogen bond (HN Aib[12]–CO Leu[8], Aib[9]), which was restrained by eight restraints (by two upper and two lower on each bond) increased by 0.2 Å relatively to restraints for a usual hydrogen bond.

Structure refinement and Monte Carlo (MC) simulations were carried out using the FANTOM program (von Freyberg and Braun, 1991) with the ECEPP/2 force field (Nemethy et al., 1983) and the same distance, hydrogen bond, and torsion angle restraints as in the DYANA's calculations. In MC simulation, an implicit solvation model with atomic solvation parameters (ASP), derived for gas-water, gas-octanol, and gas-cyclohexane transfer (Efremov et al., 1999), was used. Distance-dependent dielectric permeability $\varepsilon = r$ was employed, where r is a distance.

Visual analysis of the obtained structures, calculation of a helix bending angle, and estimation of solvent accessible surface area were performed using the MOLMOL program (Koradi et al., 1996).

PDB accession code

The refined spatial structure of Zrv-IIB contained the simultaneously present bifurcated hydrogen bond HN Aib[12]–CO Leu[8], Aib[9] (24 models ranked by energy with total energy (ECEPP/2 energy + restraints energy) lower than −65 kcal M^{-1} from 1000 starting structures) was deposited into the Protein Data Bank (http://www.rcsb.org/pdb/), accession code 1R9U.

RESULTS

Hydrogen bond pattern in Zrv-IIB in methanol solution

Usually, the existence of specific hydrogen bonds is inferred indirectly from spatial proximity of the donor and acceptor moieties in structures obtained by x-ray crystallography or NMR spectroscopy. In addition, solution NMR structural in-

vestigations are guided by indirect indication of hydrogen bond donors by slow hydrogen-deuterium exchange (Wuthrich, 1986) or by low temperature gradients of HN protons (Baxter and Williamson, 1997). In our previous work, we relied on these homonuclear NMR data and came to the conclusion that all HN protons from HN Ile[5] to the C-terminus of the peptide, except HN Aib[14], are hydrogen bonded. After searching for appropriate acceptors, we decided that the N-terminus of the peptide is completely α-helical, and the C-terminal part of the molecule has a mixed $3_{10}/\alpha$-type hydrogen bond pattern (Balashova et al., 2000).

Now, using long-range HNCO experiment (Cordier and Grzesiek, 1999), we can measure the values of $^{3h}J_{NC'}$ (scalar couplings across hydrogen bonds) and directly detect presence or absence of specific hydrogen bond. The long-range HNCO spectrum and, proposed on its basis, hydrogen bond pattern are shown on the Fig. 1; the measured values of $^{3h}J_{NC'}$ are shown on the Fig. 3. The observed pattern in general coincides with one suggested on the basis of homonuclear NMR experiments only. However, there are several differences and surprises.

The N-terminus of the peptide starts from the α-helical hydrogen bond between CO Ac[0] and HN Iva[4]. Although the long-range crosspeak for this connectivity is partially overlapped (in $\omega1$ direction) with the sequential crosspeak from HN Iva[4] (Fig. 1), we quantified it using the procedure of line-shape integration in the program XEASY. Earlier we did not suppose that HN Iva[4] can play a role of a hydrogen bond donor since it exchanges rapidly with solvent deuterons (Fig. 2) (Balashova et al., 2000), but the line-shape analysis definitely showed the participation of this amide proton in the hydrogen bond formation. At the same time, the line-shape analysis of the overlapped (in $\omega2$ direction) crosspeaks from HN Gln[3] and HN Trp[1] showed that HN Gln[3] (with a lower temperature coefficient than HN Iva[4]) has a coupling constant through a possible hydrogen bond with CO Ac[0] lower than a detection limit of 0.05 Hz.

In addition, we found that HN Aib[14] is hydrogen bonded with CO Gln[11], in spite of fast exchange with the solvent, and HN Phl[16] forms with CO Hyp[13], the 3_{10}-type hydrogen bond, rather than an α-type hydrogen bond with CO Aib[12] as we supposed earlier (Balashova et al., 2000).

In that way, the peptide is completely α-helical from its N-terminus to Leu[8], whereas the C-terminus of molecule is stabilized by 3_{10}-type hydrogen bonds. One should note that a similar hydrogen bond pattern was observed in crystal structures of homologs to Zrv-IIB peptaibols, namely Leu[1]-zervamicin (Karle et al., 1991, 1994) and antiamoebin (Snook et al., 1998; Karle et al., 1998).

The most interesting feature of the Zrv-IIB long-range HNCO spectrum is the presence of two weak hydrogen bond crosspeaks from HN Aib[12] (with associated couplings constants of −0.09 and −0.08 Hz) corresponding to the bifurcated hydrogen bond with CO Leu[8] and CO Aib[9]. The appearance of these crosspeaks is illustrated on 1D slices
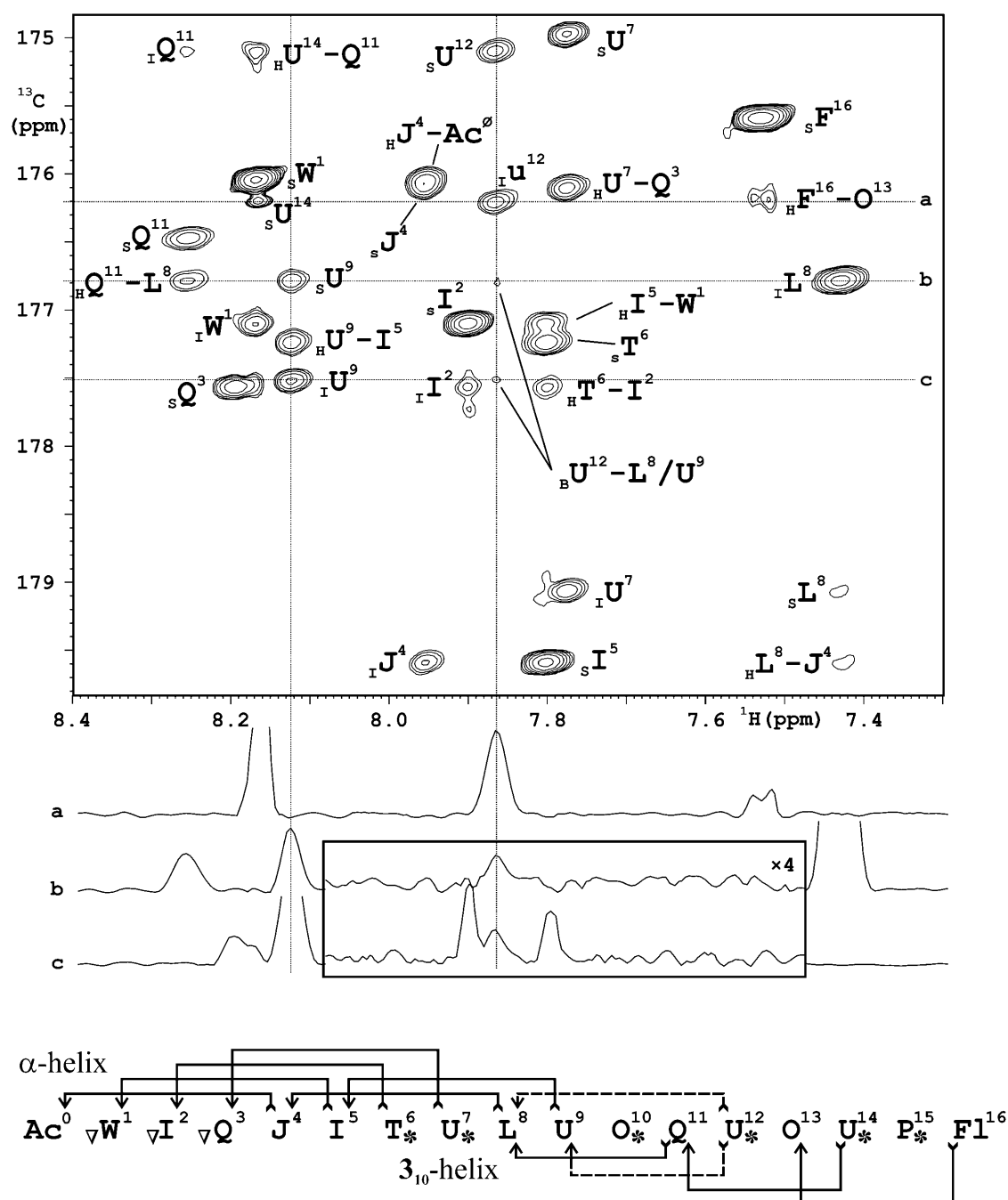
FIGURE 1 Long-range HNCO spectrum of 4 mM Zrv-IIB in CD$_3$OH (apparent pH 6.2; 305 K). Peaks are labeled by one letter amino acid code, where Acetyl, Aib, Iva, Hyp, and Phl are abbreviated as Ac, U, J, O, and F, respectively, and other residues as usual. Peaks also subdivided in four classes: (I) denotes intraresidual connectivity through $^2J_{NC'}$ coupling constant; (S) denotes sequential connectivity through $^1J_{NC'}$ coupling constant; (H) denotes long-range connectivity through $^{3h}J_{NC'}$ (across hydrogen bond) coupling constant; and (B) denotes bifurcated hydrogen bond connectivity. For categories H and B, all participant residues are listed. The respective 1D slices for bifurcated hydrogen bond connectivities and for reference signals are labeled a, b, and c and shown at the bottom of the two-dimensional spectrum. The vertical scale is identical for all slices, excluding expanded regions that are magnified vertically four times. (*Lower panel*) Hydrogen bond pattern, based on long-range HNCO spectrum. The hydrogen bonds are subdivided on α-helical and 3$_{10}$-helical; the dashed lines show the bifurcated hydrogen bond from HN Aib^{12}. The exposed (nonhydrogen-bonded) backbone amide protons are denoted by triangles; the exposed carbonyls are denoted by asterisks.
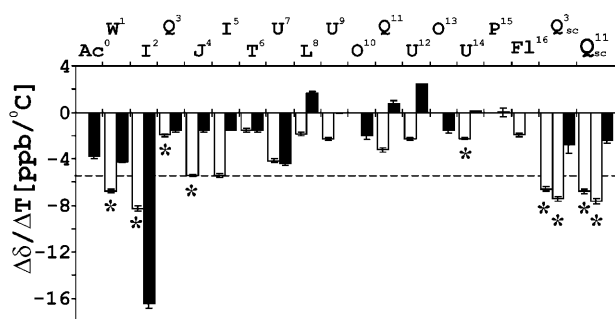
FIGURE 2 Temperature coefficients (*ppb/K*) for amide protons (*solid bars*) and carbonyl carbons (*open bars*) chemical shifts in Zrv-IIB in methanol (apparent pH 6.2; temperature range 280–320 K). Dashed line on −5.5-ppb/K level approximately divides hydrogen bonded and free amide protons (except nonbonded HN Gln[3]). Asterisks denote rapidly exchanging with solvent amide protons.

FIGURE 3 Values of $^{3h}J_{NC'}$ coupling constants (*Hz*) across hydrogen bonds (*open bars*) versus exchange contribution to transverse ^{15}N relaxation times (s^{-1}) (*solid bars*) in the corresponding hydrogen bond donor site (data taken from Korzhnev et al., 2001). Hydrogen bonds that are influenced by exchange process are indicated on the top of the figure.

(Fig. 1); although the peaks are weak, their amplitudes are two times larger than the maximal noise level. The bifurcated hydrogen bonds (with one hydrogen bond donor and two acceptors) were never observed in the crystal structures of homologs to Zrv-IIB peptaibols and, to our knowledge, were never before detected by NMR in proteins. The low values of associated $^{3h}J_{NC'}$ couplings may arise from the specific geometry of two hydrogen bonds formed simultaneously or from the dynamics exchange between two hydrogen bond acceptors that is fast on the NMR timescale.

Zrv-IIB also contains another bifurcated hydrogen bond, which shares one acceptor (CO Leu[8]) for two donors (HN Gln[11] and Aib[12]) and represents usual bifurcated hydrogen bond, frequently found in proteins. For example, the large survey of hydrogen bonding in protein crystal structures indicates that 35.5% of CO groups form simultaneously more than one hydrogen bond, but at the same time only 4.2% of HN groups are capable to form bifurcated hydrogen bond (Baker and Hubbard, 1984).

The transhydrogen bonds scalar couplings versus other NMR techniques for hydrogen bond detection

The values of transhydrogen bonds scalar couplings (Fig. 3) have direct relationship to the length of a hydrogen bond and consequently to its strength (Cordier and Grzesiek, 1999; Cornilescu et al., 1999). That is why it is interesting to compare the observed values of $^{3h}J_{NC'}$ with other parameters that are frequently used as indicators of hydrogen bond formation, namely temperature coefficients of amide protons and carbonyl carbons chemical shifts (Fig. 2.) and amide protons exchange rates.

As expected (Alexandrescu et al., 2001), we did not find any apparent correlation between these four parameters. It is not surprising because the rate of hydrogen-deuterium
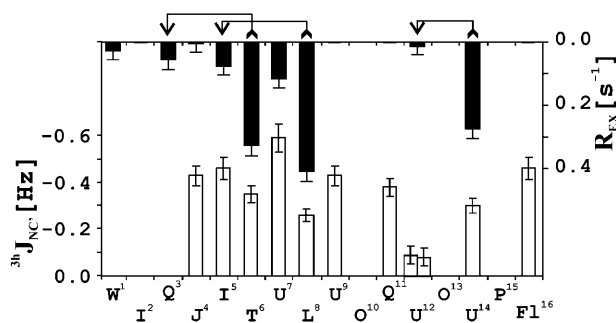
exchange can be influenced by solvent exposure, local pH, charge distributions, and dynamics of peptide (Wuthrich, 1986; Jaravine et al., 2000). In turn, the temperature coefficient of an amide proton chemical shift is expected to depend upon hydrogen bonding to solvent (Rothemund et al., 1996; Baxter and Williamson, 1997). Therefore, we should use such data for the suggestion of possible hydrogen bonds very carefully. However, it worth noting that a simple rule for identification of hydrogen bonds donors in proteins (Baxter and Williamson, 1997) works excellent in our case (if we move the temperature coefficient threshold to −5.5 ppb/K, dividing the bonded and nonbonded HN groups). Namely, the amide proton that exchanges rapidly and demonstrates a temperature coefficient less than −5.5 ppb/K should be considered as nonhydrogen bonded. Conversely, the proton that exchanges slowly and has a temperature coefficient larger than −5.5 ppb/K is hydrogen bonded.

The temperature coefficients of carbonyl carbons chemical shifts do not show any significant correlation with $^{3h}J_{NC'}$, and it was generally expected since carbonyl chemical shift depends upon hydrogen bonding in a complex way (Llinas et al., 1977; de Dios and Oldfield, 1994; Kameda et al., 1996; Wishart and Case, 2001). For example, the strongly bonded carbonyl of Ile[2] demonstrates the largest coefficient of about −16 ppb/K. At the same time, measurements of $^{3h}J_{NC'}$ repeated at the elevated temperature (315 K) indicate that the transhydrogen bond coupling for CO Ile[2] remains the same within an experimental error (data not shown). Therefore, the large coefficient of Ile[2] does not indicate that CO Ile[2] is hydrogen nonbonded or the temperature dependent disruption of a corresponding hydrogen bond but rather demonstrates a ring-current shift from the side chain of Trp[1] or an indirect effect from the hydrogen bonding of HN Gln[3] to solvent, which also depends on temperature. This absence of correlation should warn against using CO temperature coefficients of chemical shifts as indicators of a hydrogen bond acceptor.

Strength of intramolecular hydrogen bonds in Zrv-IIB helix: implications for understanding dynamic behavior of the peptide

J coupling constants across hydrogen bonds have pronounced dependence from bond length (Cornilescu et al., 1999) and from other geometrical parameters (Scheurer and Bruschweiler, 1999; Barfield, 2002). For example, the mean $^{3h}J_{NC'}$ value in β-strand regions (where hydrogen bonds are generally shorter; Baker and Hubbard, 1984) of protein ubiquitin is -0.65 vs. -0.38 Hz in α-helical regions (Cordier and Grzesiek, 1999). On the other hand, $^{3h}J_{NC'}$ values can be substantially influenced by peptide or protein dynamics (Markwick et al., 2003) and by collective polarization of hydrogen bond chains in proteins (Juranic et al., 2002). A recent example showed that values of couplings through partially populated hydrogen bonds depend linearly on the population of the bonded state. If one changes these populations, for example, by addition of trifluoroethanol, the values of associated coupling constants are changed too (Jaravine et al., 2001).

The mean value of $^{3h}J_{NC'}$ for helical Zrv-IIB (except a bifurcated bond involving NH Aib[12]) is -0.41 ± 0.09 Hz (Fig. 3). Such large values indicate that isolated helix of Zrv-IIB have stability comparable with helices of globular proteins. The conclusion about high Zrv-IIB stability is also confirmed by recent dynamical investigation of ^{15}N labeled Zrv-IIB (Korzhnev et al., 2001). The generalized order parameters for subnanosecond timescale motions for backbone HN groups were found to have the values ~0.8 that are typical for stable protein regions.

Nevertheless, the values of $^{3h}J_{NC'}$ are not uniformly distributed along the Zrv-IIB sequence. There is a strip of slightly lowered $^{3h}J_{NC'}$ lying on a polar face of the molecule (Fig. 3). Comparison of the results presented here with the aforementioned investigation of Zrv-IIB dynamics and especially with exchange contribution to ^{15}N transverse relaxation rate R_{EX} (Fig. 3) indicates that the hydrogen bond donors associated with the weakest $^{3h}J_{NC'}$ in Zrv-IIB (HN Thr[6], HN Leu[8] and HN Aib[14] (excluding HN Aib[12])) coincide with the sites with the largest R_{EX} contributions.

Let us suppose that this exchange process involves some distortions of hydrogen bonds on a polar face of Zrv-IIB. Such distortions (rearrangement of hydrogen bond pattern, opening-closure of individual hydrogen bond, or lengthening-shortening motions of individual hydrogen bond) should influence chemical shifts of not only the ^1HN donor protons but also of the ^1HN protons that lie in the same peptide plane with the hydrogen bond accepting CO group (Llinas and Klein, 1975). The change in chemical shift between different states is a necessary condition for observation of chemical exchange by NMR. Indeed, the HN Gln[3], HN Ile[5], and HN Aib[12] that lie in the same peptide planes with acceptors of the weakest hydrogen bonds (with the donors HN Thr[6], HN

Leu[8], and HN Aib[14]) demonstrate small (but significant) R_{EX} contributions (Fig. 3).

The nature of this exchange process may be quite complicated, but recent investigation of line-width concentration dependence in Zrv-IIB and in its spin-labeled analog (Z. O. Shenkarev, unpublished) indicates the absence of specific intermolecular interactions between polar faces of Zrv-IIB helices in methanol solution. Therefore, we propose that this process is inherent to isolated Zrv-IIB monomer in solution.

In principle, several types of exchange processes can lead to experimentally observed phenomena (R_{EX} and lowered values of $^{3h}J_{NC'}$). First, the helix bending motions, which are inherent to peptaibol helices (North et al., 1994; Gibbs et al., 1997; Sessions et al., 1998; Jacob et al., 1999; Tieleman et al., 2001b), can lead to lengthening-shortening motions of an individual hydrogen bond on a polar face of the helix, diminish values of $^{3h}J_{NC'}$, and (in case of slow motions) produce significant R_{EX}. Second, one can not disregard the possibility of hydrogen bonds switching between different acceptors (for example, α-3_{10} switching) or, moreover, disruption of the intramolecular hydrogen bonds with exposure of amide protons to solvent. Probably just the last mechanism plays a role in the exchange associated with HN Aib[14], since this amide proton exchanges rapidly with solvent deuterons. In this respect, it is interesting to note that the donor of the bifurcated hydrogen bond HN Aib[12] has small R_{EX} contribution (Fig. 3). From this observation, one can assume that two hydrogen bond crosspeaks from HN Aib[12] are not related to dynamical switching between two usual hydrogen bonds, but represent a true bifurcated hydrogen bond formed simultaneously.

The remaining sites of the large R_{EX} contributions HN Aib[7] and HN Trp[1] are possibly originated by the same, as mentioned above, exchange process on a polar face of the helix and by exchange with solvent, respectively.

The exchange process(es) in the Zrv-IIB helix does not deny the statement about high stability of the Zrv-IIB helix in methanol solution. The measured values of $^{3h}J_{NC'}$ indicate that fluctuations of the Zrv-IIB structure (if any) are transient in nature, and properly folded helical Zrv-IIB represents the major form of Zrv-IIB in solution.

High helix stability in methanol solution is atypical for peptaibols. For example, molecular dynamics simulations and NMR investigation of spin labeled analogs of the long peptaibol alamethicin showed that the helix of this peptaibol in methanol solution is capable of bending in large degree with disruption of $\alpha/3_{10}$-type hydrogen bonds and formation of unusual γ- or π-type bonds in the middle of the molecule (North et al., 1994; Gibbs et al., 1997; Sessions et al., 1998; Jacob et al., 1999). On the basis of our data, we should exclude the possibility of such large structural fluctuations for the Zrv-IIB helix. Probably Zrv-IIB is fairly rigid in a proposed hinge region, near Hyp[10], and consequently does not possess large amplitude hinge bending motions.

Structure refinement

Knowledge of hydrogen bond pattern in solution and information about hydrogen bonds length should significantly enhance precision and accuracy of NMR spatial structures. However, inclusion of hydrogen bond restraints in usual protocols for structure calculation is quite difficult. The hydrogen bonds restraints cannot readily be expressed in terms of distance and angle restraints due to a complex dependence of $^{3h}J_{NC'}$ from geometry (Cornilescu et al., 1999; Scheurer and Bruschweiler, 1999; Barfield, 2002) and protein dynamics (Jaravine et al., 2001; Markwick et al., 2003).

Therefore, we restrained each experimentally determined pair of hydrogen bond partners in a uniform fashion (see Materials and Methods). The constraints for each nonbifurcated hydrogen bond were included in structure calculation using the DYANA program and in subsequent energy minimization within the FANTOM program. To reveal the possible presence of the bifurcated hydrogen bond between HN Aib[12] and CO Leu[8], and CO Aib[9], and classify the mode of bifurcation (switching of acceptors versus a simultaneously present bifurcated hydrogen bond), three independent runs of structure calculation/energy minimization were carried out. In the first (I) and the second (II) runs, this hydrogen bond was restrained with the same usual distance restraints as a nonbifurcated one: either (I) α-helical bond HN Aib[12]–CO Leu[8] or (II) 3_{10}-helical bond HN Aib[12]–CO Aib[9]. In the third run (III), this bond was constrained as a bifurcated one with simultaneous but loosened restraints from both CO groups (see Materials and Methods).

The results of energy minimization crucially depend on the employed solvent model and on the way of treatment of the Coulomb potential (Efremov et al., 1999). Therefore, to find correct ECEPP/2 force field parameters for structure refinement, the ASPs for water, octanol, or cyclohexane (Efremov et al., 1999) and several dielectric permeability constants were tested. In each case, short (15,000 random steps) MC simulation starting from the DYANA structure was performed. A hydrogen bond pattern in the set of best conformations from each MC run was analyzed. The results showed that in energy minimum the model peptide adopts the conformation, similar to that observed in the experiment, in case of cyclohexane ASPs and distance-dependent dielectric permeability $\varepsilon = r$, where r is distance. Therefore, we used these parameters in all subsequent calculations.

To achieve exhaustive sampling of the conformation space, each structure calculation run (I, II, and III) was started from 1000 random structures. After that, in each run, the 420 best (with the lowest target function) structures were taken and subjected to energy minimization. Finally, the 20 best (the lowest energy) structures, obtained in each run, were analyzed and compared. The results of spatial structure calculation and subsequent energy minimization are summarized in Table 1.

As seen in Table 1, in all three runs, the DYANA structures have almost identical target function values, and one cannot choose more favorable conformation around HN Aib[12] based on these calculations. At the same time, the energy minimization results are significantly different; in average, the conformation with bifurcated hydrogen bond is energetically more favorable by 10 kcal M^{-1}. As seen in Table 1, the energy difference comes from the ECEPP/2 force field but not from the experimental restraints. Such an energy difference would lead to significant overpopulation of the conformation with a bifurcated hydrogen bond over the conformation with a nonbifurcated one, and convinces us that in methanol solution the HN Aib[12] forms the bifurcated hydrogen bond with CO Leu[8] and Aib[9] simultaneously.

The 24 best structures from run III (with total energy < -65 kcal M^{-1}) were taken as an ensemble that represents the most populated Zrv-IIB structure in solution. All these structures contain the bifurcated hydrogen bond and fit the experimental data in the best way (maximal distance violation is 0.11 Å). The structural statistics for this ensemble are presented in Table 2, and these structures are shown in Fig. 4 A. Low DYANA target function and backbone root mean-square deviation (rmsd) values for the low energy structures (Table 2) along with very abundant experimental restraints illustrate high precision of the determined structure.

The refined structure of Zrv-IIB in methanol solution presented here substantially differs from structures determined previously in methanol (Balashova et al., 2000; PDB code 1DLZ) and in solution of DPC micelles (Shenkarev et al., 2002; PDB code 1IH9) (rmsd between ensembles of structures are 0.82 Å and 0.94 Å, respectively). However, several qualitative structural features draw together the refined structure of the peptide in methanol solution and in DPC micelles. First, the hydrogen bond between CO Ac[0] and HN Iva[4] and participation of HN Aib[14] in hydrogen bonding were suggested in the course of the structure determination in DPC micelles. Second, in the structure presented here, the angle of helix bending on Hyp[10] is only 20°, which better corresponds to the angle of bending in DPC micelles (~23°), rather than one in methanol solution, incorrectly determined earlier (~43°).

We can consider the close similarity between the peptide structures in different media (including preservation of the helix bending angle) as an additional definite proof of the high rigidity of the Zrv-IIB helix. However, in several crystal forms of Leu[1]-Zrv, the angle of bending varies between 47° and 26° (Karle et al., 1991, 1994), which may be an outcome of crystal packing forces. Earlier this fact was considered as an evidence for flexibility of zervamicin in the hinge region. Summarizing all the up-to-date experimental data, we suppose that Zrv-IIB has a well-defined angle of the helix bending (~20°) in different environments but can change it upon transition to extreme conditions, as illustrated by crystallization.

TABLE 1 Statistics for three cycles of DYANA structure calculation/FANTOM energy minimization for different acceptors of hydrogen bond from HN Aib[12]

		α-Helical	3_{10}-Helical	Bifurcated
The best 420 DYANA structures				
DYANA target function (Å^2)	Mean	0.070	0.066	0.084
	SD	0.022	0.013	0.04
	Max	0.28	0.13	0.29
Backbone rmsd (Å^2)		0.17	0.38	0.20
The best 20 FANTOM structures				
FANTOM total energy (ECEPP/2 energy + restraints energy) (kcal M^{-1})	Mean	−50.9	−52.6	−68.0
	SD	5.8	3.5	2.0
	Min	−63.2	−61.5	−72.4
ECEPP/2 energy (kcal M^{-1})	Mean	−55.5	−58.2	−72.0
	SD	5.5	3.9	2.6
	Min	−67.01	−66.1	−77.3
Backbone rmsd (Å^2)		0.29	0.32	0.18

Interaction with solvent of the Zrv-IIB helix

Based on the observed hydrogen bonds, we can enumerate all the nonhydrogen bonded backbone polar groups in Zrv-IIB. These groups are depicted by triangles and stars (HN and CO, respectively) in Fig. 1. As proposed earlier (Shenkarev et al., 2002), the C-terminus of the Zrv-IIB helix is more polar than the N-terminus (four nonbonded CO versus three nonbonded HN groups). In addition, there are two nonbonded carbonyls of Thr[6] and Aib[7] in the center of the molecule. Such distribution of polar regions on the surface of the Zrv-IIB helix might be essential for its functioning. There are a number of speculations about participation of the exposed carbonyls in ion conductance and about nonequivalence of N- and C-termini manifested in asymmetry of voltage gating of peptaibols (Fox and Richards, 1982; Sansom, 1991; Sansom et al., 1993; Wallace, 2000).

The nonparticipation of CO group in intramolecular hydrogen bonding does not denote solvent exposure and formation of strong hydrogen bonds with solvent molecules. Therefore, to investigate interaction of Zrv-IIB with solvent, we should use other NMR indicators of CO hydrogen bonding. In principal, each peptide plane contains several such indicators, for example, a chemical shift of amide proton (Llinas and Klein, 1975; Juranic et al., 1995) and a direct coupling constant $^1J_{NC'}$ across the peptide bond (Juranic et al., 1995, 2002). Finally, we can resort to our highly refined structure. As shown above, this structure represents major solution state of Zrv-IIB, and we can estimate solvent accessible surface area of carbonyl oxygens from the obtained structures.

In helical peptides, the ^{1}HN chemical shifts depend on conformation (Asakura et al., 1995; Wishart and Case, 2001) and can identify the helix-end effects (Wishart and Sykes, 1994), hydrogen bonding of the HN and CO group within

TABLE 2 Structural statistics for the 24 representative structures of Zrv-IIB in methanol solution

| Parameter	Unit	Quantity	Value
ECEPP/2 energy	Kcal M^{-1}	Average ± SD	−71.2 ± 3.0
DYANA target function	Å^2	Average ± SD	0.98 ± 0.01
No. of distance constraints		NOE (upper/lower)	125/16
		H-bond (upper/lower)	22/22
No. of torsion angle constraints		Angle ϕ	8
		Angle χ^1	4
Upper constraint violations	Å	Sum ± SD	1.10 ± 0.10
		Maximum	0.11
Lower constraint violations	Å	Sum ± SD	0.10 ± 0.00
		Maximum	0.08
Van der Waals constraint violations	Å	Sum ± SD	0.00 ± 0.00
		Maximum	0.03
Angle constraint violations	Degrees	Sum ± SD	0.00 ± 0.00
		Maximum	0.00
Rmsd of atom coordinates (residues 0–16)	Å	Backbone	0.13 ± 0.04
		All heavy atoms	1.12 ± 0.33
Length of helix (C$^\alpha$Ac^0–C'Phl^{16})	Å	From–to (in the ensemble)	25.1–25.6
Angle of bending on Hyp^{10}	Degrees	From–to (in the ensemble)	19.8–23.4

NOE, nuclear Overhauser effect.
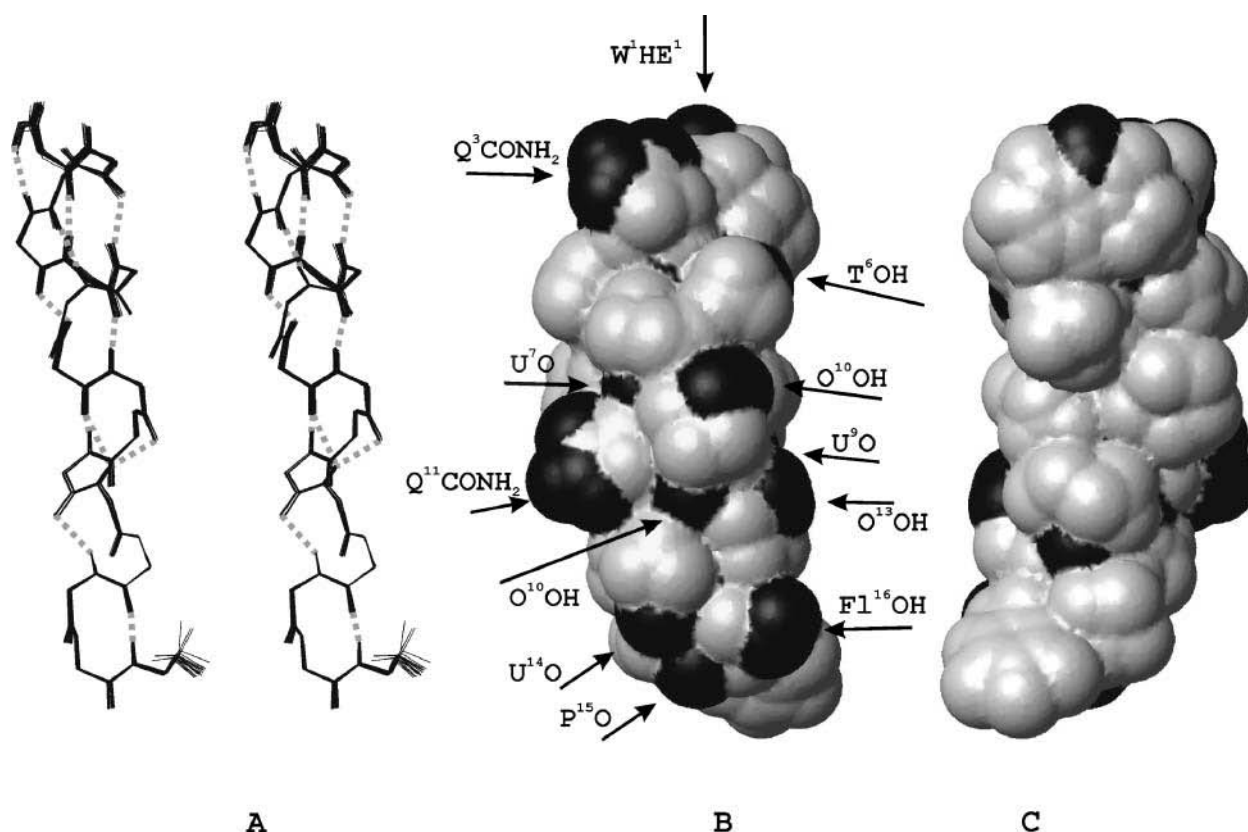
FIGURE 4 (*A*) Stereo view of the 24 best structures of Zrv-IIB in methanol solution. Only the backbone of the molecule is shown. Hydrogen bonds are indicated by shaded dashed lines. (*B*) Surface representation of a polar (convex) face of the Zrv-IIB helix. The surfaces of the polar groups are shown in black. The groups that contribute to these regions are signed. Orientation of the molecule is the same as in *A*. (*C*) Surface representation of a nonpolar (concave) face of the Zrv-IIB helix. Orientation of the molecule differs from *B* by 180°.

one peptide plane (Llinas and Klein, 1975; Juranic et al., 1995), and various distortions from the ideal helical structure, including kinks and curving (Blanco et al., 1992). The amide protons secondary shifts $\Delta\delta^1HN$ ($\delta^{HN}-\delta^{HN}_{RC}$) are summarized in Fig. 5 *A*. (Please note that there is no experimental or statistical study of the random coil ^1HN chemical shifts for Aib and Iva residues; therefore, we arbitrary chose these shifts equal to 8.40 ppm, although the random coil ^1HN chemical shifts for Aib and Iva residues should be different.) As we can see from Fig. 5 *A*, all the HN groups in Zrv-IIB have negative secondary shifts as expected for helical conformation. As a demonstration of helical-end effect, the N-terminal (Trp[1]) and C-terminal (Phl[16]) residues in Zrv-IIB have the most positive and the most negative $\Delta\delta^1HN$, respectively. However, the Leu[8] HN proton is deshielded on approximately the same level as HN Phl[16]; moreover, the $\Delta\delta^1HN$ steadily go down from HN Trp[1] to HN Leu[8] (Fig. 5 *A*). This observation can be rationalized, if we imagine that although the helix of the peptide is not interrupted on the Leu[8], the free carbonyls of Thr[6] and Aib[7] polarize the middle of the helix, thus producing pseudo-C-terminus. Such behavior was expected for peptaibols; for example, alamethicin has a similar pattern of HN chemical

shifts (Yee et al., 1995). The behavior of other ^1HN chemical shifts in the N-terminal region (Trp[1]–Leu[8]) is strongly dominated by this helix-end effect, and taking into account the arguments of Blanco et al. (1992), we can consider this region as a regular α-helix. At the same time, the pattern of $\Delta\delta^1HN$ at the C-terminus of the peptide is characteristic of an irregular helix with kinks, as expected for the sequence with an alternation of Pro/non-Pro residues (Blanco et al., 1992).

Direct coupling constants across the peptide bond $^1J_{NC'}$ in Zrv-IIB have uniform values with an average of -15.0 ± 0.8 Hz (Fig. 5 *B*), as expected for helices (Juranic et al., 1995). The $^1J_{NC'}$ for the N- and C-terminal residues stand out from others constants, because of the helical-end effect. In general, the values of $^1J_{NC'}$ are slightly less than 15 Hz in the N-terminal part and slightly higher in the C-terminal part of the peptide. This indicates an overall increase in hydrogen bonding of CO groups with solvent in the C-terminal part of the peptide as compared with the N-terminal part. On the other hand, uniform distribution of $^1J_{NC'}$ values, without any prominent values, indicates that hydrogen bonds with solvent of the free carbonyls of Thr[6], Aib[7], and Hyp[10] have the strength comparable with the strength of intermolecular hydrogen bonds.
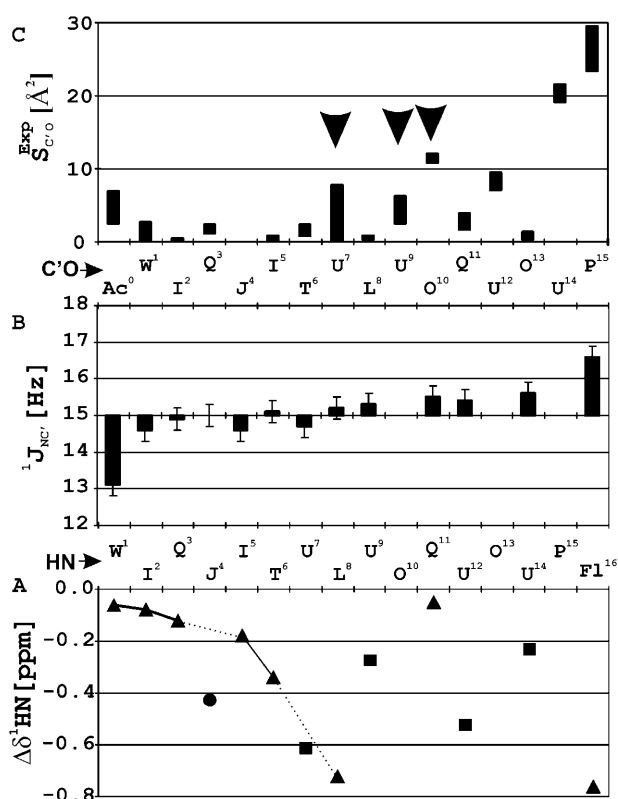
FIGURE 5 (A) Amide protons secondary shifts $\Delta\delta^1HN$ ($\delta^{HN}-\delta^{HN}_{RC}$) for Zrv-IIB in methanol solution. Values for usual residues are denoted by triangles. The $\Delta\delta^1HN$ for Aib and Iva residues (*squares* and *circles*, respectively) are calculated with assumption that δ^{HN}_{RC} is equal to 8.40 ppm, although δ^{HN}_{RC} for Aib and Iva obviously should be different. The values in the N-terminus are connected by lines to emphasize the tendency. (B) Direct coupling constants across peptide bond $^1J_{NC'}$ (*Hz*). The values for Pro/Hyp containing peptide planes were not determined. (C) Solvent accessible surface areas for carbonyl oxygens in the refined Zrv-IIB structure in methanol solution. The solid bars designate the ranges of exposed surfaces adopted in the set of the 24 best structures. The variability of the values for N- and C-termini and Aib[7] in the middle of the helix indicates the reduced structural order in these regions. The arrows designate exposed carbonyls, which form a hydrophilic patch.

Estimated from the set of the 24 best structures, solvent accessible surface areas for carbonyl oxygens are summarized on the Fig. 5 C. All nonbonded carbonyls (except CO Thr[6]) have a large (>6 Å^2 in the set of the 24 best structures) exposed surface. In the central part of the peptide, three exposed carbonyls of Aib[7], Aib[9], and Hyp[10] (Fig. 5 C) significantly enhance the polar face of the amphiphilic molecule and, along with the side chains of Hyp[10], Gln[11], and Hyp[13], form a polar patch (Fig. 4 B). If the channel of Zrv-IIB is formed by a bundle of parallel helices (in a manner proposed by Sansom et al., 1993), then rings of exposed carbonyls (along with polar side-chain groups) can form the site of dehydration of monovalent cations moving through the pore and can underlie the cation selectivity of Zrv-IIB channels (Kropacheva and Raap, 2002). The similar sites are observed in others cation-selective ion channels: bacterial

K$^+$ channels KcsA, MthK, and KvAp (Doyle et al., 1998; Jiang et al., 2002a, 2003a), and the peptide antibiotic gramicidin A (Golovanov et al., 1991). The solvent accessible surfaces for exposed CO groups from these channels, along with surfaces for exposed CO groups from the peptaibols alamethicin and Zrv-IIB, are summarized in Table 3. As illustrated by this table, the modes of solvent interaction in the Zrv-IIB and alamethicin helices are different. Alamethicin has one significantly exposed carbonyl of Gly[11] in the middle of the helix, which strongly interacts with solvent in methanol solution (Fox and Richards, 1982; Yee et al., 1997). At the same time, Zrv-IIB in the central part of the helix has three exposed CO groups (Aib[7], Aib[9], and Hyp[10]) with moderate (<15 Å^2) exposure to solvent (Fig. 5 C). This agrees well with the observed pattern of $^1J_{NC'}$.

A polar patch on a convex face of the Zrv-IIB helix (formed by backbone carbonyls and polar side chains; see Fig. 4 B) in methanol solution is significantly large than in alamethicin in the same milieu (Fox and Richards, 1982; Yee et al., 1997). Keeping in mind the unusual, for peptaibols, stability of the Zrv-IIB helix and complete preservation of the peptide structure upon transition to anisotropic micelle environment, we propose that a mode of Zrv-IIB/solvent interaction is preserved at least in membrane surface bound form. If the active channel of Zrv-IIB is formed by a bundle of, at the minimum, four parallel helices (Sansom et al., 1993), the polar patches from different monomers face the pore of channel. And if the mode of solvent/peptide interactions remains the same upon transition to the transmembrane state, the enlarged polar patch should lead to altered cation-peptide interactions in the channel bundle and consequently could alter pore selectivity.

This, indeed, takes place. The selectivity pattern for the lowest conductance level of alamethicin (K$^+$ > Na$^+$) (Hanke and Boheim, 1980) differs from the selectivity pattern of Zrv-IIB in vesicular system (Na$^+$ > K$^+$) (Kropacheva and Raap, 2002). Although these patterns were measured in different experiments (in artificial planar lipid membrane and in vesicular system), we believe that the results are comparable, as in each case only low conductance states were measured. In the planar lipid bilayer, the selectivity was observed only for the lowest conductance level (tetrameric bundle; Tieleman et al., 2002) of alamethicin; the larger bundles did not exhibited any selectivity. At the same time, as estimated from peptide/lipid ratio in vesicular experiments, each vesicle contained only three to nine Zrv-IIB molecules (Kropacheva and Raap, 2002); such a number of monomers can form two conductance aggregates with lowest conductance levels (tetrameric bundle; Sansom et al., 1993) or one larger bundle. Statistically in a huge number of vesicles, there was a bulk of smallest aggregates to demonstrate Na$^+$ selectivity, but there was also a nonnegligible quantity of larger aggregates, and we can argue that the actual Na$^+$/K$^+$ permeability rate is more than 2.0 (the value was measured by Kropacheva and Raap,

2002). Thus, we propose that the structure of Zrv-IIB and especially peptide/solvent interactions underlie the peptaibol selectivity toward alkali cations.

CONCLUSION

This study shows that the short peptaibol Zrv-IIB structure significantly differs from long peptaibols. First of all, Zrv-IIB in methanol solution forms a rigid kinked helix, stabilized by a network of hydrogen bonds with strength comparable with that of hydrogen bonds in the helical regions of globular proteins, whereas long peptaibols alamethicin (Yee et al., 1995) and chrysospermin C (Anders et al., 1998) demonstrate rapid equilibrium between several conformations in methanol solution.

A polar face of the amphiphilic Zrv-IIB helix is formed by a continuous strip of polar side chains and exposed backbone carbonyls (with moderate exposure to solvent in methanol solution) (Figs. 4 B and 5 C), whereas in alamethicin and chrysospermin (in the crystal and micellar environment, respectively; Fox and Richards, 1982; Anders et al., 2000), the polar face is dominated by significantly exposed carbonyl of Gly^{11}(Ala^{11}), which (in the case of alamethicin) strongly interacts with solvent in methanol solution (Yee et al., 1997).

In this way, according to our voltage-gated (pre)orientation-insertion model for peptaibol action (Shenkarev et al., 2002), we can speculate about two different structural paradigms for peptaibols that act via the barrel-stave mechanism.

Long peptaibols, represented by alamethicin, have 18–20 residues in length, which are sufficient to span the hydrocarbon region of the bilayer in α-helical conformation. In addition, they are able to afford helix-bending motions, which decrease the dipole moment of the helix, but in spite of that, they are the most active peptaibols (Duclohier and Wroblewski, 2001). On the contrary, short peptaibols, represented by zervamicin, have 14–16 residues in length. To span the membrane and act according to the barrel-stave

mechanism, the short peptaibols should adopt a large quantity of 3_{10}-helix (that is longer than α-helix). Also the short peptaibols should be more rigid and linear in the hinge region, to maintain maximal dipole moment. The conductance properties of alamethicin (Sansom, 1991) and zervamicins (Balaram et al., 1992) illustrate that different structural paradigms lead to approximately the same activity in the bilayer.

The deviations from these two structural paradigms result in diminished activity and unmask other (nonbarrel-stave) mechanisms of action. As an example, one could mention the peptaibol antiamoebin I (Snook et al., 1998) and the lipo-peptaibol trichogin GA IV (Kropacheva and Raap, 2002). The first one (antiamoebin) is homologous to Zrv-IIB, but its N-terminal part is very mobile, as illustrated by completely different conformations in solid and solution states (right-handed versus left-handed helix) (Galbraith et al., 2003). The second one (trichogin) is too short (11 residues) to span the membrane.

The fact that the types of peptaibol-solvent interactions in two peptaibol families are different either could be a consequence of structural differences between two paradigms or could denote two different concepts developed by nature in the design of amphiphilic helices. In the last case, the different modes of helix-solvent interaction were differently realized in two families only accidentally.

The recent developments in the crystallography of bacterial potassium channels (Doyle et al., 1998; Jiang et al., 2002a, 2003a) provide a better understanding into the following question: Are peptaibols appropriate models for cell voltage-gated channels? It is obvious that transient peptaibols pores differ significantly from large channels and have an unlike mechanism of voltage gaiting. In spite of that, nature employs several similar structural approaches in the designing of these two classes of channels:

1. The overall structural organization in both cases is a helical bundle (Doyle et al., 1998; Tieleman et al., 2002).

TABLE 3 Solvent accessible surface areas (SASA) of exposed carbonyls from ion channels (in the case of several available values the maximum is listed)

Molecule structure	Biological role	CO group	SASA (Å^2)
Bacterial K$^+$ channel KcsA. X-ray structure, PDB entry 1BL8 (Doyle et al., 1998)	Selective filter	Thr^{75}	19.4
		Val^{76}	21.9
		Gly^{77}	25.1
		Tyr^{78}	29.7
Gramicidin A. Peptide antibiotic. NMR structure, PDB entry 1GRM (Arseniev et al., 1985)	Dehydration of monovalent cations, site of divalent cation binding, selective filter (Golovanov et al., 1991)	D-Leu^{10}	10.0
		D-Leu^{12}	19.3
		D-Leu^{14}	19.4
Zrv-IIB. Peptaibol antibiotic. NMR structure, PDB entry 1R9U (this work)	Dehydration of cations?	Aib^7	7.8
		Aib^9	6.2
		Hyp^{10}	12.0
Alamethicin. Peptaibol antibiotic. X-ray structure, PDB entry 1AMT (Fox and Richards, 1982)	Dehydration of cations?	Aib^{10}	6.0
		Gly^{11}	18.5

2. Both peptide and protein molecules have exposed backbone carbonyls that participate in ion conductance through the pore (Balaram et al., 1992; Doyle et al., 1998).

3. The event that underlies voltage gaiting is a reorientation of a helical rigid body under action of external electric field (Tieleman et al., 2001a; Jiang et al., 2003b).

4. The hinge-bending motion opens the pore in the potassium channel and plays crucial role in peptaibol ion conductance (Jacob et al., 1999; Jiang et al., 2002b).

It should be emphasized that in peptaibols all of these functions are realized in the same helix, whereas large potassium channels have distinct structural regions (domains) for selectivity filter, voltage sensor, and pore.

REFERENCES

Alexandrescu, A. T., D. R. Snyder, and F. Abildgaard. 2001. NMR of hydrogen bonding in cold-shock protein A and an analysis of the influence of crystallographic resolution on comparisons of hydrogen bond lengths. *Protein Sci.* 10:1856–1868.

Anders, R., O. Ohlenschlager, V. Soskic, H. Wenschuh, B. Heise, and L. R. Brown. 2000. The NMR solution structure of the ion channel peptaibol chrysospermin C bound to dodecylphosphocholine micelles. *Eur. J. Biochem.* 267:1784–1794.

Anders, R., H. Wenschuh, V. Soskic, S. Fischer-Fruhholz, O. Ohlenschlager, K. Dornberger, and L. R. Brown. 1998. A solution NMR study of the selectively 13C, 15N-labeled peptaibol chrysospermin C in methanol. *J. Pept. Res.* 52:34–44.

Argoudelis, A. D., A. Dietz, and L. E. Johnson. 1974. Zervamicins I and II, polypeptide antibiotics produced by Emericellopsis salmosynnemata. *J. Antibiot. (Tokyo).* 27:321–328.

Arseniev, A. S., I. L. Barsukov, V. F. Bystrov, A. L. Lomize, and Y. Ovchinnikov. 1985. 1H-NMR study of gramicidin A transmembrane ion channel. Head-to-head right-handed, single-stranded helices. *FEBS Lett.* 186:168–174.

Asakura, T., K. Taoka, M. Demura, and M. P. Williamson. 1995. The relationship between amide proton chemical shifts and secondary structure in proteins. *J. Biomol. NMR.* 6:227–236.

Baker, E. N., and R. E. Hubbard. 1984. Hydrogen bonding in globular proteins. *Prog. Biophys. Mol. Biol.* 44:97–179.

Balaram, P., K. Krishna, M. Sukumar, I. R. Mellor, and M. S. Sansom. 1992. The properties of ion channels formed by zervamicins. *Eur. Biophys. J.* 21:117–128.

Balashova, T. A., Z. O. Shenkarev, A. A. Tagaev, T. V. Ovchinnikova, J. Raap, and A. S. Arseniev. 2000. NMR structure of the channel-former zervamicin IIB in isotropic solvents. *FEBS Lett.* 466:333–336.

Barfield, M. 2002. Structural dependencies of interresidue scalar coupling h3JNC′ and donor 1H chemical shifts in the hydrogen bonding regions of proteins. *J. Am. Chem. Soc.* 124:4158–4168.

Barranger-Mathys, M., and D. S. Cafiso. 1996. Membrane structure of voltage-gated channel forming peptides by site-directed spin-labeling. *Biochemistry.* 35:498–505.

Bartels, C., T. Xia, M. Billiter, P. Guntert, and K. Wuthrich. 1995. The program XEASY for computer-supported NMR spectral analysis of biological macromolecules. *J. Biomol. NMR.* 6:1–10.

Baumann, G., and P. Mueller. 1974. A molecular model of membrane excitability. *J. Supramol. Struct.* 2:538–557.

Baxter, N. J., and M. P. Williamson. 1997. Temperature dependence of 1H chemical shifts in proteins. *J. Biomol. NMR.* 9:359–369.

Blanco, F. J., J. Herranz, C. Gonzalez, M. A. Jimenez, M. Rico, J. Santoro, and J. L. Nieto. 1992. NMR chemical shifts: a tool to characterize distortions of peptide and protein helices. *J. Am. Chem. Soc.* 114:9676–9677.

Clubb, R. T., V. Thanabal, and G. Wagner. 1992. A constant-time three-dimensional triple-resonance pulse scheme to correlate intraresidue 1HN, 15N, and 13C′ chemical-shifts in 15N-13C′-labeled proteins. *J. Magn. Reson.* 97:213–217.

Cordier, F., and S. Grzesiek. 1999. Direct observation of hydrogen bonds in proteins by interresidue 3hJNC′ scalar couplings. *J. Am. Chem. Soc.* 121:1601–1602.

Cornilescu, G., B. E. Ramirez, K. Frank, G. M. Clore, A. M. Gronenborn, and A. Bax. 1999. Correlation between 3hJNC′ and hydrogen bond length in proteins. *J. Am. Chem. Soc.* 121:6275–6279.

de Dios, A. C., and E. Oldfield. 1994. Chemical shifts of carbonyl carbons in peptides and proteins. *J. Am. Chem. Soc.* 116:11485–11488.

Doyle, D. A., C. J. Morais, R. A. Pfuetzner, A. Kuo, J. M. Gulbis, S. L. Cohen, B. T. Chait, and R. MacKinnon. 1998. The structure of the potassium channel: molecular basis of K+ conduction and selectivity. *Science.* 280:69–77.

Duclohier, H., and H. Wroblewski. 2001. Voltage-dependent pore formation and antimicrobial activity by alamethicin and analogues. *J. Membr. Biol.* 184:1–12.

Efremov, R. G., D. E. Nolde, G. Vergoten, and A. S. Arseniev. 1999. A solvent model for simulations of peptides in bilayers. I. Membrane-promoting alpha-helix formation. *Biophys. J.* 76:2448–2459.

Emsley, L., and G. Bodenhausen. 1989. Gaussian pulse cascades: new analytical functions for rectangular selective inversion and in-phase excitation in NMR. *Chem. Phys. Lett.* 165:469–476.

Fox, R. O., and F. M. Richards. 1982. A voltage-gated ion channel model inferred from the crystal structure of alamethicin at 1.5-A resolution. *Nature.* 300:325–330.

Franklin, J. C., J. F. Ellena, S. Jayasinghe, L. P. Kelsh, and D. S. Cafiso. 1994. Structure of micelle-associated alamethicin from 1H NMR. Evidence for conformational heterogeneity in a voltage-gated peptide. *Biochemistry.* 33:4036–4045.

Galbraith, T. P., R. Harris, P. C. Driscoll, and B. A. Wallace. 2003. Solution NMR studies of antiamoebin, a membrane channel-forming polypeptide. *Biophys. J.* 84:185–194.

Gibbs, N., R. B. Sessions, P. B. Williams, and C. E. Dempsey. 1997. Helix bending in alamethicin: molecular dynamics simulations and amide hydrogen exchange in methanol. *Biophys. J.* 72:2490–2495.

Golovanov, A. P., I. L. Barsukov, A. S. Arseniev, V. F. Bystrov, S. V. Sukhanov, and L. I. Barsukov. 1991. The divalent cation-binding sites of gramicidin A transmembrane ion-channel. *Biopolymers.* 31:425–434.

Grzesiek, S., and A. Bax. 1992. Improved 3D triple-resonance NMR techniques applied to a 31-kDa protein. *J. Magn. Reson.* 96:432–440.

Guntert, P., C. Mumenthaler, and K. Wuthrich. 1997. Torsion angle dynamics for NMR structure calculation with the new program DYANA. *J. Mol. Biol.* 273:283–298.

Hanke, W., and G. Boheim. 1980. The lowest conductance state of the alamethicin pore. *Biochim. Biophys. Acta.* 596:456–462.

He, K., S. J. Ludtke, H. W. Huang, and D. L. Worcester. 1995. Antimicrobial peptide pores in membranes detected by neutron in-plane scattering. *Biochemistry.* 34:15614–15618.

Jacob, J., H. Duclohier, and D. S. Cafiso. 1999. The role of proline and glycine in determining the backbone flexibility of a channel-forming peptide. *Biophys. J.* 76:1367–1376.

Jaravine, V. A., A. T. Alexandrescu, and S. Grzesiek. 2001. Observation of the closing of individual hydrogen bonds during TFE-induced helix formation in a peptide. *Protein Sci.* 10:943–950.

Jaravine, V. A., K. Rathgeb-Szabo, and A. T. Alexandrescu. 2000. Microscopic stability of cold shock protein A examined by NMR native state hydrogen exchange as a function of urea and trimethylamine N-oxide. *Protein Sci.* 9:290–301.

Jiang, Y., A. Lee, J. Chen, M. Cadene, B. T. Chait, and R. MacKinnon. 2002a. Crystal structure and mechanism of a calcium-gated potassium channel. *Nature.* 417:515–522.

Jiang, Y., A. Lee, J. Chen, M. Cadene, B. T. Chait, and R. MacKinnon. 2002b. The open pore conformation of potassium channels. *Nature.* 417:523–526.

Jiang, Y., A. Lee, J. Chen, V. Ruta, M. Cadene, B. T. Chait, and R. MacKinnon. 2003a. X-ray structure of a voltage-dependent K+ channel. *Nature.* 423:33–41.

Jiang, Y., V. Ruta, J. Chen, A. Lee, and R. MacKinnon. 2003b. The principle of gating charge movement in a voltage-dependent K+ channel. *Nature.* 423:42–48.

Juranic, N., P. K. Ilich, and S. Macura. 1995. Hydrogen bonding networks in proteins as revealed by the amide 1JNC′ coupling constant. *J. Am. Chem. Soc.* 117:405–410.

Juranic, N., M. C. Moncrieffe, V. A. Likic, F. G. Prendergast, and S. Macura. 2002. Structural dependencies of h3JNC′ scalar coupling in protein H-bond chains. *J. Am. Chem. Soc.* 124:14221–14226.

Kameda, T., N. Takeda, S. Kuroki, H. Kurosu, S. Ando, I. Ando, A. Shoji, and T. Ozaki. 1996. Hydrogen-bonded structure and 13C NMR chemical shift tensor of amino acid residue carbonyl carbons of peptides and polypeptides in the crystalline state. Part I. *J. Mol. Struct.* 384:17–23.

Karle, I. L., J. L. Flippen-Anderson, S. Agarwalla, and P. Balaram. 1991. Crystal structure of [Leu1]zervamicin, a membrane ion-channel peptide: implications for gating mechanisms. *Proc. Natl. Acad. Sci. USA.* 88:5307–5311.

Karle, I. L., J. L. Flippen-Anderson, S. Agarwalla, and P. Balaram. 1994. Conformation of the flexible bent helix of Leu1-zervamicin in crystal C and a possible gating action for ion passage. *Biopolymers.* 34:721–735.

Karle, I. L., M. A. Perozzo, V. K. Mishra, and P. Balaram. 1998. Crystal structure of the channel-forming polypeptide antiamoebin in a membrane-mimetic environment. *Proc. Natl. Acad. Sci. USA.* 95:5501–5504.

Koradi, R., M. Billeter, and K. Wuthrich. 1996. MOLMOL: a program for display and analysis of macromolecular structures. *J. Mol. Graph.* 14:51–55, 29–32.

Korzhnev, D. M., E. V. Bocharov, A. V. Zhuravlyova, V. Y. Orekhov, T. V. Ovchinnikova, M. Billeter, and A. S. Arseniev. 2001. Backbone dynamics of the channel-forming antibiotic zervamicin IIB studied by 15N NMR relaxation. *FEBS Lett.* 495:52–55.

Kropacheva, T. N., and J. Raap. 1999. Voltage-dependent interaction of the peptaibol antibiotic zervamicin II with phospholipid vesicles. *FEBS Lett.* 460:500–504.

Kropacheva, T. N., and J. Raap. 2002. Ion transport across a phospholipid membrane mediated by the peptide trichogin GA IV. *Biochim. Biophys. Acta.* 1567:193–203.

Llinas, M., and M. P. Klein. 1975. Charge relay at the peptide bond. A proton magnetic resonance study of solvation effects on the amide electron density distribution. *J. Am. Chem. Soc.* 97:4731–4737.

Llinas, M., D. M. Wilson, and M. P. Klein. 1977. Peptide hydrogen bonding. Conformation dependence of the carbonyl carbon-13 nuclear magnetic resonance chemical shifts in ferrichrome. A study by 13C-[15N] Fourier double resonance spectroscopy1a. *J. Am. Chem. Soc.* 99:6846–6850.

Marion, D., M. Ikura, R. Tschudin, and A. Bax. 1989. Rapid recording of 2D NMR spectra without phase cycling. Application to the study of hydrogen exchange in proteins. *J. Magn. Reson.* 85:393–399.

Markwick, P. R., R. Sprangers, and M. Sattler. 2003. Dynamic effects on j-couplings across hydrogen bonds in proteins. *J. Am. Chem. Soc.* 125:644–645.

Nemethy, G., M. S. Pottle, and H. A. Scheraga. 1983. Energy parameters in polypeptides. 9. Updating of geometrical parameters, nonbonded interactions, and hydrogen bond interactions for the naturally occurring amino acids. *J. Phys. Chem.* 87:1883–1887.

North, C. L., J. C. Franklin, R. G. Bryant, and D. S. Cafiso. 1994. Molecular flexibility demonstrated by paramagnetic enhancements of nuclear relaxation. Application to alamethicin: a voltage-gated peptide channel. *Biophys. J.* 67:1861–1866.

Ovchinnikova, T. V., Z. O. Shenkarev, Z. A. Yakimenko, N. V. Svisheva, A. A. Tagaev, D. A. Skladnev, and A. S. Arseniev. 2003. Biosynthetic uniform 13C,15N-labeling of zervamicin IIB. Complete 13C and 15N NMR assignment. *J. Pept. Sci.* 9:817–826.

Rothemund, S., H. Weisshoff, M. Beyermann, E. Krause, M. Bienert, C. Mugge, B. D. Sykes, and F. D. Sonnichsen. 1996. Temperature coefficients of amide proton NMR resonance frequencies in trifluoroethanol: a monitor of intramolecular hydrogen bonds in helical peptides. *J. Biomol. NMR.* 8:93–97.

Sansom, M. S. 1991. The biophysics of peptide models of ion channels. *Prog. Biophys. Mol. Biol.* 55:139–235.

Sansom, M. S., P. Balaram, and I. L. Karle. 1993. Ion channel formation by zervamicin-IIB. A molecular modelling study. *Eur. Biophys. J.* 21:369–383.

Scheurer, C., and R. Bruschweiler. 1999. Quantum-chemical characterization of nuclear spin-spin couplings across hydrogen bonds. *J. Am. Chem. Soc.* 121:8661–8662.

Sessions, R. B., N. Gibbs, and C. E. Dempsey. 1998. Hydrogen bonding in helical polypeptides from molecular dynamics simulations and amide hydrogen exchange analysis: alamethicin and melittin in methanol. *Biophys. J.* 74:138–152.

Shaka, A. J., P. B. Barker, and R. Freeman. 1985. Computer-optimized decoupling scheme for wideband applications and low-level operation. *J. Magn. Reson.* 64:547–552.

Shenkarev, Z. O., T. A. Balashova, R. G. Efremov, Z. A. Yakimenko, T. V. Ovchinnikova, J. Raap, and A. S. Arseniev. 2002. Spatial structure of zervamicin IIB bound to DPC micelles: implications for voltage-gating. *Biophys. J.* 82:762–771.

Snook, C. F., G. A. Woolley, G. Oliva, V. Pattabhi, S. F. Wood, T. L. Blundell, and B. A. Wallace. 1998. The structure and function of antiamoebin I, a proline-rich membrane-active polypeptide. *Structure.* 6:783–792.

Tieleman, D. P., H. J. Berendsen, and M. S. Sansom. 2001a. Voltage-dependent insertion of alamethicin at phospholipid/water and octane/water interfaces. *Biophys. J.* 80:331–346.

Tieleman, D. P., B. Hess, and M. S. Sansom. 2002. Analysis and evaluation of channel models: simulations of alamethicin. *Biophys. J.* 83:2393–2407.

Tieleman, D. P., I. H. Shrivastava, M. R. Ulmschneider, and M. S. Sansom. 2001b. Proline-induced hinges in transmembrane helices: possible roles in ion channel gating. *Proteins.* 44:63–72.

von Freyberg, B., and W. Braun. 1991. Efficient search for all low energy conformations of polypeptides by Monte Carlo methods. *J. Comp. Chem.* 12:1065–1076.

Wallace, B. A. 2000. Common structural features in gramicidin and other ion channels. *Bioessays.* 22:227–234.

Wishart, D. S., and D. A. Case. 2001. Use of chemical shifts in macromolecular structure determination. *Methods Enzymol.* 338:3–34.

Wishart, D. S., and B. D. Sykes. 1994. Chemical shifts as a tool for structure determination. *Methods Enzymol.* 239:363–392.

Wuthrich, K. 1986. NMR of Proteins and Nucleic Acids. John Wiley and Sons, New York.

Yee, A. A., R. Babiuk, and J. D. O. Neil. 1995. The conformation of an alamethicin in methanol by multinuclear NMR spectroscopy and distance geometry/simulated annealing. *Biopolymers.* 36:781–792.

Yee, A. A., K. Marat, and J. D. O'Neil. 1997. The interactions with solvent, heat stability, and 13C-labelling of alamethicin, an ion-channel-forming peptide. *Eur. J. Biochem.* 243:283–291.